Turbulence effects on wind flow over complex terrain

Michael Sherry, John Sheridan, David Lo Jacono

17th Australasian Fluid Mechanics Conference
Auckland, New Zealand
5-9 December 2010

Turbulence effects on wind flow over complex terrain

M. Sherry [1], **J. Sheridan** [1] **and D. Lo Jacono** [1,2,3]

[1]Fluids Laboratory for Aerospace and Industrial Engineering, Department of Mechanical and Aerospace Engineering, Monash University, Victoria, 3800, Australia

[2]Université de Toulouse; INPT, UPS; IMFT; Allée Camille Soula, F-31400 Toulouse, France.

[3] CNRS; IMFT; F-31400 Toulouse, France

Abstract

Flow separation experiments over a forward facing step immersed in a turbulent boundary layer subjected to various levels of freestream turbulence intensity have been undertaken in a water channel. Freestream turbulence was generated using two traditional grids and a third, novel tethered sphere design, which was shown to dramatically increase the turbulence intensity produced. Planar particle image velocimetry was used to characterise the mean recirculation region. The dynamic of the reattachment length was also investigated using instantaneous velocity realisations. It was found that bluff body geometry effects were dominant over the freestream turbulence intensity close to the separation point. Downstream of the separation point, the turbulence level was seen to increase mixing between the high momentum freestream flow and the adverse flow within the recirculation region promoting reattachment.

Introduction

Wind turbines are now an established method of generating eco-friendly electricity. With the rapid expansion of the wind industry in the last decade, suitable flat terrain with a favourable wind resource is becoming scarce. Wind turbines are therefore commonly sited in complex topography such as cliffs and escarpments to take advantage of the wind speed up effects the topography produces. However, flow separation occurs in complex terrain causing increased wind shear and turbulence intensity, both of which may reduce turbine life expectancy. The current one-dimensional models used in the design of wind farm sites are unable to predict where flow separation occurs.

To investigate the flow field over a cliff/escarpment, a model forward facing step (FFS) immersed in a turbulent boundary layer was investigated in a water channel. Sherry et al. [8], found the mean reattachment length, X_L is sensitive to a number of parameters such as the boundary layer δ, to step height h ratio and the Reynolds number, Re_h. It is also known for flow over a blunt flat plate that freestream turbulence levels affect the surface pressure distribution and the mean reattachment length [7, 1]. Here, the effect of freestream turbulence intensity, I_u, defined as the ratio of the root mean square of the fluctuating streamwise velocity component and the mean streamwise velocity was investigated using a number of passive turbulence grids. A novel tethered sphere design was also tested to improve isotropy of the turbulence generated [9]. The turbulence intensity ranges from the minimum of approximately 1.45% with no grid in place to 9.9% with the tethered grid.

The purpose of the current study was to investigate the effect of freestream turbulence intensity and length scale on the flow field downstream of a forward facing step.

Experimental Method

The free surface water channel has a working section of $600 \times 800 \times 4\,000$mm and a working speed range of $0.09\,\text{m/s} < U_\infty < 0.46\,\text{m/s}$. The channel walls are constructed of glass allowing easy optical access. Flow uniformity is achieved through the use of an upstream honeycomb section and fine turbulence screen. The flow passes through a 3:1 contraction to accelerate the mean flow and reduce the residual streamwise turbulence intensity to 1.45%.

The experiments were conducted over a Reynolds number range of $6\,531 < Re_h < 7\,371$. The Reynolds number is defined as $Re_h = U_\infty\, h\, /\nu$, where U_∞ is the free stream velocity, h is the step height, and ν is the kinematic viscosity of the working fluid. In the current tests the step height was fixed at $h = 30$mm. Additional turbulence screens where utilised were placed $8.34h$ and $28.34h$ upstream of the model leading edge and forward facing step edge respectively.

A CCD Particle Image Velocimetry (PIV) camera with a resolution of $4\,008 \times 2\,672$ pixels was used in conjunction with a 105 mm lens to acquire the velocity fields. A multi-step interrogation window with an initial size of 64×64 pixels to a final size of 32×32 pixels with 50% overlap was used. This allowed instantaneous velocity maps of 250 by 167 vectors to be captured.

A total of 500 independent image pairs were captured for each Reynolds number and grid setting. Whilst the recirculation zones presented were all the result of averaging of the turbulent flow, convergence (via variance of the fluctuating cross velocity product from the cumulative mean) was shown to occur prior to 500 image pairs. Therefore 500 images pairs were deemed an acceptable compromise between convergence of the results and excessive use of disk space. The raw data was processed on a 20 CPU (Beowulf) cluster that allowed rapid analysis of results. Validated cross correlation PIV software developed in-house was employed to generate the displacement fields [2].

Turbulence Grids

Grids of various designs have been used as a method to either suppress or increase turbulence levels within experimental facilitites [5]. Three different turbulence grid designs were used in the current study, their properties can be seen in table 1. The mesh size, M, and the solidity ratio, σ, are known to influence the turbulence intensity and scale produced by the grids [5]. As the turbulence is only generated at the grid itself, it decays with streamwise distance from the grid. One particular feature of grid generated turbulence is that it is anistropic with deviations in the streamwise direction larger than those in the spanwise and wall normal directions. To improve the isotropy and increase the turbulence intensity generated, a novel tethered sphere design was tested [9]. This design utilised a conventional passive turbulence grid and tethered spheres to improve mixing and hence isotropy of the turbulence generated. The spheres were constructed of celluloid ('table tennis') balls of diameter 38mm, which were filled with water to minimise buoyancy effects. Our

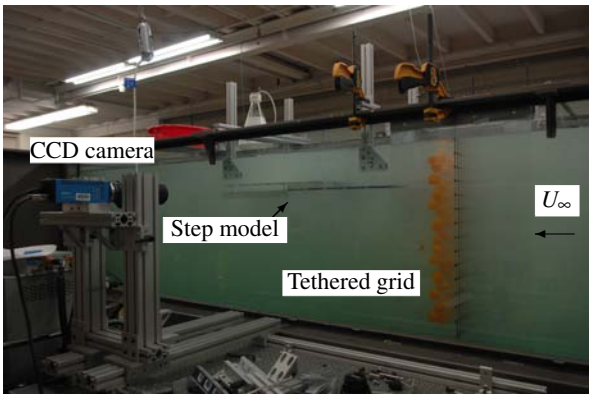

Figure 1: Experimental setup showing the tethered sphere turbulence grid upstream of forward facing step model in the FLAIR water channel

Turbulence properties				
	No Grid	Grid 1	Grid 2	Grid 3
Mesh size	-	$0.42h$	$1.67h$	$1.67h$
Solidity	-	22%	41%	41%*
Intensity (I_u)	1.45	1.85	3.18%	9.9%

Table 1: Turbulence properties of the four flow settings simulated in the current study. Grid 1: plain small mesh, Grid 2: plain large mesh, Grid 3: tethered sphere grid

grid design used a sphere diameter, D, to mesh size ratio, D^* of 0.76, shown to produce the largest turbulence intensity [9]. The tether lengths, L^* varied from 1.5–2D to ensure freedom of movement arising from vortex induced vibration of the tethered spheres. Figure 1 shows the tethered grid located upstream of the experimental model in the water channel.

A 2D TSI Laser Doppler Velocimeter (LDV) was used to accurately characterise the turbulence generated by the various grids. The effect of the tethered sphere grid is shown in table 1 to have a three fold increase in turbulence intensity. *The solidity ratio of the tethered sphere grid shown in table 1 is based on the grid support structure, an alternate solidity ratio could be defined based on the projected area of the spheres, this value is 72%.

Results

The recirculation zone dimensions using the PIV results were determined by calculating the streamfunction (see equation 1), above the step surface.

$$u = \frac{\delta\psi}{\delta y}, \psi = \int_0^y (\overline{u}/U_\infty)\mathrm{d}(y/h), \qquad (1)$$

where $\overline{u}$ is the temporal average of the streamwise velocity component. **Equation 1 is an accurate estimation of the streamfunction due to the non-propagating error in the streamwise direction [6].**

For the data analysis, the Cartesian coordinate system was fixed at the step leading edge. The mean reattachment length, X_L, is defined by the point where the dividing streamline, $\psi = 0$, (from here on denoted as ψ_0) bifurcated at the step surface and the region of negative flow ceases. At the reattachment point, one arm of the dividing streamline returns upstream into the recirculation region and the second continues downstream. The height of the recirculation region, Y_b is defined as the maximum height of the dividing streamline above the step.

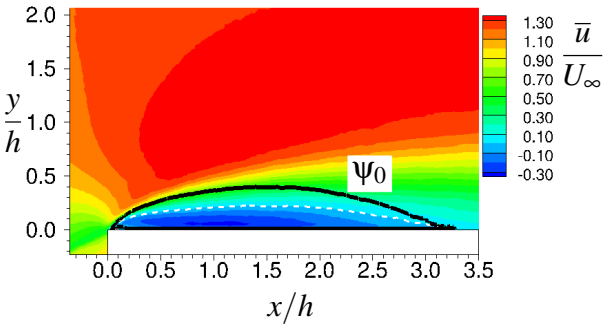

Figure 2: General bluff body flow features of the FFS flow in a low turbulence freestream flow, contours of mean streamwise velocity $\overline{u}$; solid line is the dividing streamline ψ_0, dashed white line encapsulates region of entirely negative flow, $\delta/h = 1.35$, $I_u = 1.45\%$, $Re_h = 7371$.

The isocontours of the mean streamwise velocity, $\overline{u}$, obtained from the PIV measurements for the lowest freestream turbulence case (no grid) are shown in figure 2, where the Reynolds number, Re_h is 7371 and the turbulence intensity I_u is 1.45%. The flow is from left to right, with the length and velocity scales non dimensionalised against the step height, h, and freestream velocity, U_∞, respectively. The region of maximum velocity speed up ($\overline{u}/U_\infty = 1.3$) can be seen by the red contour above the step. This region is beneficial in an ideal wind energy sense. The recirculation region is indicated by the solid line (ψ_0), while the white dashed contour line encapsulates the region of entirely negative flow. The white dashed line also indicates the mean position of the maximum shear within the recirculation region. The mean reattachment length, X_L, and the mean height of the recirculation region, Y_b, of figure 2 are $3.24h$ and $0.396h$ respectively.

The isocontours of the mean streamwise velocity for the highest turbulence (tethered sphere grid) case are shown in figure 3. The flow direction and Reynolds number definition are the same as in figure 2. The Reynolds number, Re_h and turbulence intensity I_u of figure 3, are 6531 and 9.9%. The region of maximum velocity speed up ($\overline{u}/U_\infty = 1.2$) shown by the red contour above the step is reduced compared to figure 2 due to turbulent mixing. The recirculation region reduces in size with increased turbulence intensity. The mean reattachment length, X_L, and the mean height of the recirculation region, Y_b, of figure 3 are $2.63h$ and $0.368h$ respectively.

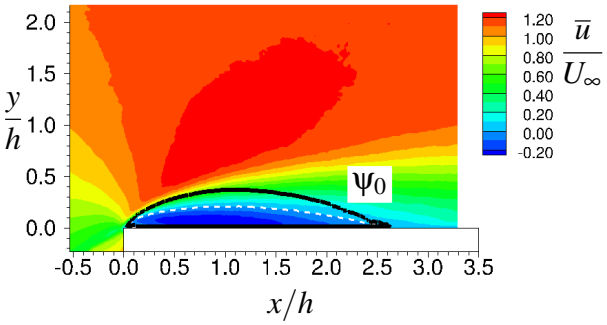

Figure 3: General bluff body flow features of the FFS flow in a high turbulent freestream flow, contours of mean streamwise velocity $\overline{u}$; solid line is the dividing streamline ψ_0, dashed white line encapsulates region of entirely negative flow, $\delta/h = 1.35$, $I_u = 9.9\%$, $Re_h = 6531$.

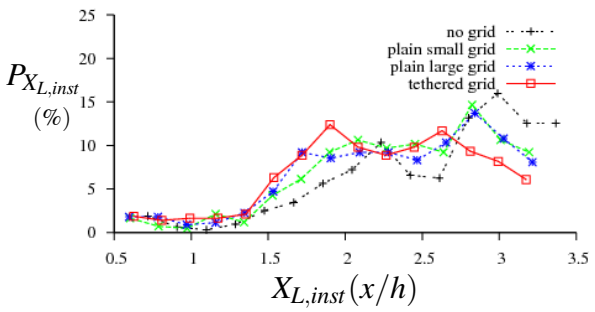

Figure 4: Probability distribution of the instantaneous reattachment positions, $X_{L,inst}$ for the four different freestream turbulence settings all with $\delta/h = 1.35$, no grid: $I_u = 1.45\%$, $Re_h = 7371$, small plain: $I_u = 1.85\%$, $Re_h = 7267$, large plain: $I_u = 3.18\%$, $Re_h = 7250$ and tethered sphere: $I_u = 9.9\%$, $Re_h = 6531$.

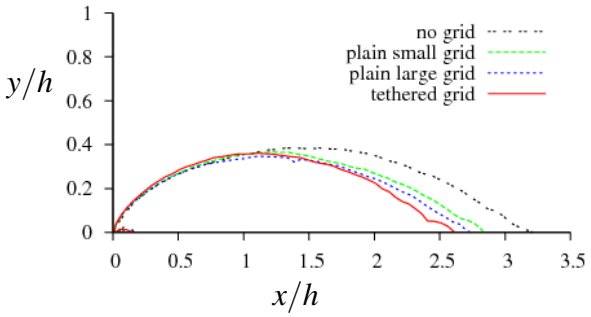

Figure 5: Recirculation region reduction with elevated freestream turbulence intensity. Recirculation region downstream of a FFS depicted by dividing streamline (ψ_0) for the four different freestream turbulence settings, U_∞ is from left to right all cases with $\delta/h = 1.35$, no grid: $I_u = 1.45\%$, $Re_h = 7371$, small plain: $I_u = 1.85\%$, $Re_h = 7267$, large plain: $I_u = 3.18\%$, $Re_h = 7250$ and tethered sphere: $I_u = 9.9\%$, $Re_h = 6531$.

To investigate the dynamics of the reattachment length, a velocity sub field close to the step top was extracted from each instantaneous PIV realisation. The height of the sub field, ($0.046h$) was outside the influence of biased data due to proximity to the wall, a common issue in PIV. A high order polynomial is fitted through the velocity data and the point at which adverse flow ceases is taken as the instantaneous reattachment position. This is a different methodology to that applied to the temporally averaged data as the instantaneous data is not steady in time. The mean reattachment location obtained from the instantaneous PIV frames is taken as the streamwise location where the maximum number of reattachments occur. A probability density function (p.d.f) of the resulting instantaneous reattachment length results is created allowing a low order estimate of the reattachment zone. The reattachment zone is estimated to occur within one standard deviation (*i.e.* 66%) of the mean instantaneous reattachment position, $\overline{X_{L,inst}}$. A p.d.f of the instantaneous reattachment locations for the different freestream turbulence intensities is shown in 4. This figure produces some interesting results in terms of the reattachment length dynamics. It appears the separated shear layer has preferred reattachment points at two distinct streamwise locations, oscillating between the two. Flow over a FFS is unsteady so one expects the broad p.d.f's shown in figure 4. The recirculation zone grows in size by entraining fluid (vorticity) from the separated shear layer until the zone cannot sustain additional fluid (vorticity) and a large scale structure (vortex) is shed downstream. It is postulated that the two peaks in the p.d.f are an indication of two of the states within this shedding process. This shedding phenomena also affects turbulent recirculation bubbles on blunt flat plates [4].

The instantaneous reattachment length results give an indication of the dynamics of the recirculation zone which cannot be seen from the temporal average as shown in figures 2 and 3. The reattachment zone increases with freestream turbulence intensity as shown in table 2.

Extracting the locus of points which make up the dividing streamline for each turbulence case produces a figure such as that shown in figure 5 for $Re_h = 7339$. The mean reattachment position, X_L, reduces by 19% as I_u increases by 85%. However the recirculation region height, Y_b, varies very little with turbulence intensity. This shows that for this variable the bluff body geometry dominates over the initial separated region. Bluff body dominance can be seen from figure 5 as the insensitivity of the initial trajectory of the separated shear layer to increased turbulence intensity. Turbulence effects become evident after the maximum vertical extent of the recirculation region where geometric influences reduce and freestream flow conditions (*e.g.* $I_u, \delta/h$) become dominant.

The mean reattachment position reduces with increasing freestream turbulence levels due to enhanced mixing between the recirculating and freestream flow allowing faster momentum recovery close to the step. It can also be seen from figure 5 and table 2 that a three fold increase in I_u only results in a 5% reduction in mean reattachment position. This could be indicative that there is a limit that is approached asymptotically on the effect of I_u. Alternatively, it could be that there is an effect due to the turbulence length scale, L_u. Due to a data sample rate restriction, the current LDV measurements have been unable to deduce the characteristic length scale of the turbulence generated by the grids. It does however form part of the ongoing work.

Summary of flow results				
	No Grid	Grid 1	Grid 2	Grid 3
I_u (%)	1.45	1.85	3.18	9.9
X_L (h)	3.24	2.87	2.76	2.62
Y_b (h)	0.396	0.374	0.354	0.368
$\overline{X_{L,inst}}$ (h)	2.9	2.8	2.8	1.9
X_L zone (h)	2.8–3.4	2.1–3.0	1.7–3.0	1.7–3.0
X_L zone width (h)	0.57	0.93	1.31	1.27

Table 2: Summary of the recirculation region dimensions with the differing freestream turbulence intensities

Reynolds stress generation

Examining the Reynolds shear stress contour plots for each turbulence setting provides useful insight into the mixing mechanisms promoting reattachment. Reynolds shear stresses are created above the step due to the turbulent motions within the flow. They are representive of the streamwise momentum flux in the wall normal-direction. Thus, a larger Reynolds shear stress component indicates more mixing (*i.e.* streamwise-momentum change vertically) caused by the fluctuating (turbulent) velocity components. Freestream turbulence causes velocity perturbations and hence one would expect a higher Reynolds shear stress component with greater freestream turbulence intensity.

Reynolds shear stress contour plots for the lowest (no grid) and highest (tethered grid) freestream turbulence levels are shown

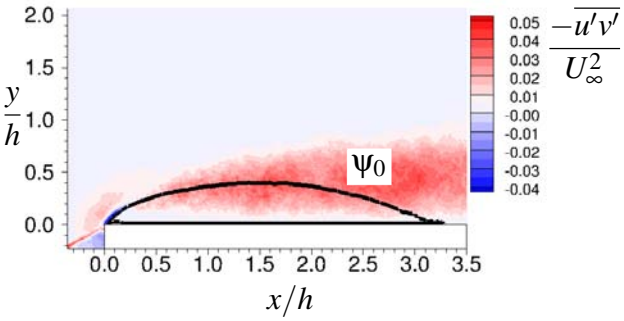

Figure 6: Reynolds shear stress contours produced above a FFS with a low freestream turbulence level $I_u = 1.45\%$, for $\delta/h = 1.35$, $Re_h = 7371$, isocontours of $-\overline{u'v'}/U_\infty^2$; solid line is the dividing streamline ψ_0

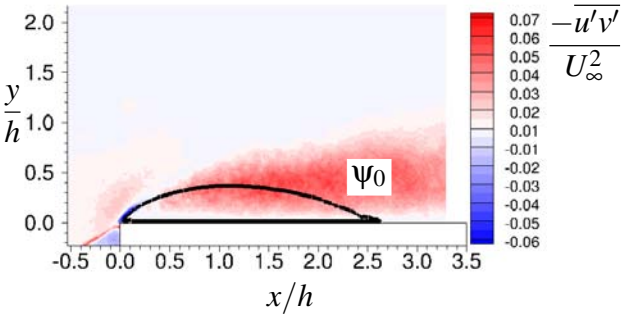

Figure 7: Reynolds shear stress contours produced above a FFS with a high freestream turbulence level $I_u = 9.9\%$, for $\delta/h = 1.35$, $Re_h = 6531$, isocontours of $-\overline{u'v'}/U_\infty^2$; solid line is the dividing streamline ψ_0

in figures 6 and 7. On first inspection, these figures appear remarkedly similar. In all turbulence cases (two not shown), negative Reynolds shear stresses are generated close to the separation point. They are an indication of the flow deflection and hence streamwise momentum flux in the positive wall-normal direction. Hattori [3] has described this region as a production region of the Reynolds shear stress component. The streamwise extent of this region changes less than ∼3% despite the freestream turbulence level increasing significantly. This is an indication of how the bluff body geometery dominates the intial region of this separating and reattaching flow.

The Reynolds shear stress component changes sign downstream of this production region when the influence of the separation point and strong velocity gradients reduce. Within the positive Reynolds shear stress region higher (freestream) streamwise momentum is being transferred toward the step to overcome the adverse flow within the recirculating region. It is in this region that the freestream turbulence will promote reattachment. Comparing figures 6 and 7, it can be seen that the Reynolds shear stress component has a larger magnitude for the tethered sphere flow results, confirming this enhanced mixing aids in reattachment. Also, qualitatively at least, the higher turbulence case (figure 7) sees faster spreading of the separated shear layer.

Conclusion

Flow separation experiments subjected to various levels of freestream turbulence intensity have been undertaken in a water channel. The freestream turbulence level was elevated by using passive turbulence grids. Two traditional grids and a third novel tethered sphere design, which was shown to dramatically increase the turbulence intensity were tested. Planar particle image velocimetry was used to characterise the mean recirculation region dimensions of the region height Y_b and length X_L. It was found that bluff body geometry effects were dominant over the freestream turbulence intensity close to the separation point. Downstream of the separation point, the freestream turbulence intensity was seen to increase Reynolds shear stress generation. It is postulated that the elevated Reynolds shear stresses increase mixing between the high momentum freestream flow and the adverse flow within the recirculation region promoting reattachment. The mean region height, Y_b, remained largely constant with increasing turbulence intensity. However, the mean reattachment length, X_L displayed a stronger relationship with the freestream turbulence level. X_L reduced by 19% with a 85% increase in the freestream turbulence intensity. The dynamics of the reattachment length were also investigated using the instantaneous PIV realisations. It was shown that the seperated shear layer reattached at two preferential streamwise locations and that the reattachment zone increased with freestream turbulence intensity.

Acknowledgements

The work of A. Kong in the data collection is greatly appreciated.

References

[1] Cherry, N., Hillier, R. and Latour, M., Unsteady measurements in a separated and reattaching flow, *Journal of Fluid Mechanics*, **144**, 1984, 13–46.

[2] Fouras, A., Lo Jacono, D. and Hourigan, K., Target-free stereo PIV: a novel technique with inherent error estimation and improved accuracy, *Experiments in fluids*, **44**, 2008, 317–329.

[3] Hattori, H. and Nagano, Y., Investigation of turbulent boundary layer over forward-facing step via direct numerical simulation. *International Journal of Heat and Fluid Flow*, **31**, 2010, 284–294.

[4] Kiya, M. and Sasaki, K., Structure of a turbulent separation bubble, *Journal of Fluid Mechanics*, **137**, 1983, 83–113.

[5] Laws, E.M. and Livesey, J.L., Flow through Screens, *Annual Review of Fluid Mechanics*, **10**, 1978, 247–266.

[6] Lo Jacono, D., Nazarinia, M., and Brons, M., Experimental vortex breakdown topology in a cylinder with a free surface, *Physics of fluids*, **21**, 111704, 2009.

[7] Saathoff, P.J. and Melbourne, W.H., Effects of free-stream turbulence on surface pressure Fluctuations in a separation bubble, *Journal of Fluid Mechanics*, **337**, 1997, 1–24.

[8] Sherry, M., Lo Jacono, D. and Sheridan, J., An experimental investigation of the recirculation region formed downstream of a forward facing step, *Submitted to Journal of Wind Engineering and Industrial Aerodynamics*, August, 2010

[9] Vonlanthen, R. and Monkewitz, P.A., A new passive turbulence grid with improved isotropy, *61st meeting of APS division of fluid dynamics*, November 25th, 2008